Orbital Mechanics & Subsystem Configurations of a Black Hole Analysing Spacecraft

Shathria Ompragash[1], Manuj Awasthi[1#] and Shane Hengst[2#]

[1]University of New South Wales, Australia
[2]University of Southern Queensland, Australia
[#]Advisor

ABSTRACT

Although invisible in the optical frequency, black holes possess an immense gravitational power capable of holding together trillions of stellar objects by acting as galactic nuclei. Scientists are currently only able to conduct indirect studies by analysing the heat-sourced X-ray emissions generated by the acceleration of surrounding matter towards the black hole singularity. Direct means of experimentation and analysis cannot be accomplished due to humankind's limited technology; moreover, the distance of separation between Earth and black holes also serves as a hindrance to the advancement of space expedition. This paper aims to provide the scientific community with foundational information to materialise a deep space satellite that will have the ability to investigate the cosmic implications initiated by the gravitational pull of a supermassive black hole. The orbital mechanics and system configurations of deep space satellites such as the Chandra X-ray Observatory, James Webb and Hubble Space Telescopes, along with the Voyager probes were critically studied. This allowed for the conceptualisation of a hypothetical deep space satellite with the potential to analyse the gravitational patterns and conduct investigations based on the theory of special relativity whilst orbiting a supermassive black hole. Features such as orbital manoeuvres and launch vehicle specifications were explored. Furthermore, an extensive study on the satellite's subsystem configuration and payload design were also conducted.

1. Introduction

In 2019, the Event Horizon Telescope (EHT) and the Chandra X-ray Observatory (CXO/ Chandra) worked collaboratively to produce radio interferometric and polarised X-ray images of the supermassive black hole (SMBH) at the centre of the Messier 87 galaxy (Figure 1A & 1B) which served as an irrefutable proof of Einstein's theory of general relativity [1]. This scientific milestone was further accentuated by the publication of the X-ray image of Sagittarius A*, the SMBH of the Milky Way galaxy in 2022 by the EHT [2] (Figure 1C).

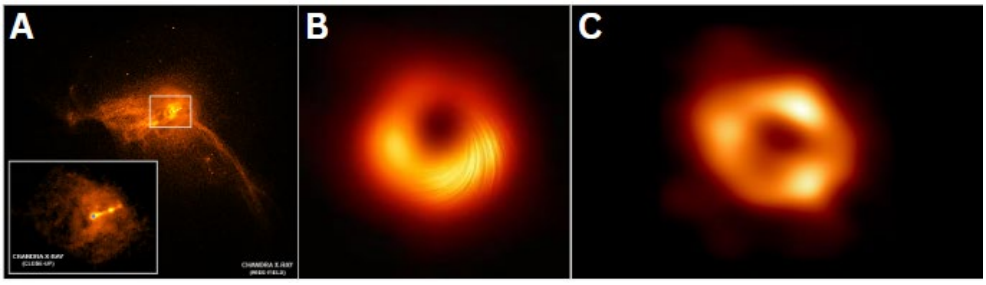

Figure 1. Interferometric images of supermassive black holes. Figure 1A shows the Messier 87 SMBH captured by the CXO in X-ray frequency [3] whilst Figure 1B shows the EHT version of the black hole in radio frequency [4]. Figure 1C depicts the Sagittarius A* SMBH captured by EHT [2] in 2022.

A black hole is defined as a region in space where the gravitational force is so powerful that nothing, including light, can escape its grasp nor communicate with the external world; they are classified into four categories: miniature (or quantum mechanical) stellar mass, intermediate and supermassive. These have been listed in ascending order of size, with the smallest weighing less than 1 $M_{\odot}$ and the largest ranging anywhere from 10^5 to 10^{10} $M_{\odot}$.

This paper aims to design a hypothetical deep space satellite equipped with the scientific instruments needed to analyse the behaviour the Sagittarius A* supermassive blackhole (SMBH). The satellite will observe the black hole in various electromagnetic frequencies and produce spectrographic images that can be analysed to understand the evolution of a black hole. Furthermore, the satellite aims to study the gravitational field patterns and the effects of special relativity near a supermassive black hole. The Satellite that Analyses Black Holes, abbreviated to STABH will carry an atomic clock to conduct experiments based on the laws of special relativity along with a magneto-gradiometer to map and analyse the gravitational wave patterns exhibited by a black hole. An array of interferometric cameras and mirrors which enable the spacecraft to obtain high resolution images of the black hole in different electromagnetic frequencies including but not limited to X-ray, radio and ultraviolet will be integrated into the payload. The subsystems of deep space satellites such as the Chandra X-ray Observatory, James Webb and Hubble Space Telescopes along with the Voyager probes were explored. The interdependency of these subsystems were studied as they determine the mission's performance and outcome, as well as the structural configuration of STABH. The subsystem analysis also assists in illustrating the relationship between the mission requirements and how they are influenced by factors such as cost, performance and lifetime demands. The analysed subsystems include (1) command and data handling, (2) power generation, storage and distribution, (3) propulsion, (4) thermal control, (5) guidance and navigation, (6) telemetry, (7) structural elements, and (8) micro-meteoroid protection.

Simulation software including Matlab and GMAT were used to design the orbital mechanics of STABH by calculating various astrophysical properties of the Sagittarius A* SMBH. A well-established game design engine (Unreal Engine 5 (UE5)) was used to simulate the satellite's orbit around the black hole by integrating the mathematics derived from Matlab and GMAT. An important aim of this mission is to construct an orbit that will allow the satellite to approach the black hole as close as possible without being overwhelmed by its gravitation. Although STABH is a hypothetical mission as the currently available propulsion technology is limited, it is expected that the analysis and discussion presented in this paper may be helpful in designing a satellite suited for the direct measurement of black hole properties should such technological advancement was to become available in the future.

This paper will focus on the Sagittarius A* supermassive black hole (SagA*) that lies at the centre of the Milky Way Galaxy, approximately 26,000 light-years (2.4599×10^{17} km) away, the mathematical solutions for a Schwarzschild black hole have been assumed for SagA*. The radius of the event horizon of a Schwarzschild black hole $R_{Sch} = \frac{2G_N M}{c^2}$ sets the threshold distance any matter can approach before being dominated by the black hole's gravitation. This will later be used in determining the orbital radius required for STABH to get as close as possible to SagA* without crossing into the event horizon.

X-ray reflection spectroscopy can be employed to study the properties of black holes. When nearby stellar objects are overpowered by the black hole's gravitation, they accelerate towards the point of singularity, approaching the event horizon. Thermally charged photons are produced by the accretion disk, indicating the presence of a hotter cloud around the black hole. This temperature variation is credited to the accelerating matter converting kinetic energy into heat energy, expelled in the form of X-ray radiation and radio waves. The disk is illuminated by the exponential cut-off in the cloud temperature in the accretion flow, this generates a reflection component. An iron Kα complex characterises the reflective emission spectrum; when observed from a distance, the thickness and distribution of these fluorescent emission lines vary due to the relativistic effects of the strong gravity region and the points of emissions in the disk [5] [6].

The subsystem design of STABH was influenced by the Chandra X-ray Observatory (Figure 2), launched in 1999. It is considered as one of the most successful deep space satellites capable of conducting X-ray spectroscopy. Orbiting at an apogee of 140,000 km and perigee of 10,000 km, Chandra employs a high-Earth elliptical trajectory [7]. Seventy percent of Chandra's 63.5-hour orbital period is dedicated to observing the cosmos. STABH will employ

a completely different orbital trajectory, however, the sequential orbit correction methods utilised by Chandra can be extrapolated for this mission, with the addition of gravity-assist transfer from the larger planets in the solar system.

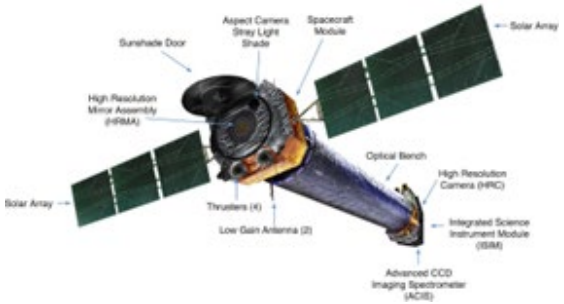

Figure 2. Structure of the Chandra X-ray Observatory [3].

Chandra's extensive ground system comprises of the Deep Space Network (DSN), the Chandra Operations Control Centre and the Chandra X-ray Centre (CXC) [8] . DSN, operated by the Jet Propulsion Laboratory has 3 antenna stations in Goldstone (California), Madrid (Spain) and Canberra (Australia). It directly communicates with Chandra by up-linking commands and down-linking telemetry data. This network acts as a bridge between Earth and Chandra situated 140,000 km away. STABH will travel a greater distance, approximately 26,000 light-years to SagA*, so the telemetry and communication system implemented in this hypothetical spacecraft requires a higher precision than CXO whilst also being able to function in deep space with limited human interference as commands and data cannot be up/downlinked instantaneously.

CXO's 4,800-kilogram graphite-epoxy structure supports a 19.5 metre deployed solar array, a High-Resolution Mirror Assembly (HRMA), Integrated Science Instruments Module (ISIM) carrying an Advanced CCD Imaging Spectrometer (ACIS) and a High Resolution Camera (HRC). The spacecraft bus module consists of the following subsystems [8]:

1. Pointing Control and Aspect Determination determines the spacecraft's attitude, solar array orientation, and momentum.
2. Communication, Command and Data Management optimises communication, storage and processing of acquired data while providing computational support. Chandra transmits information at 2250 MHz and receives at 2071.8 MHz with a command link of 2 kilobits per second (kbps).
3. The Electrical Power Subsystem generates, stores and distributes the spacecraft's primary electrical power. Two 3-panel silicon solar arrays producing 2350 W generates power whereas three 40 amp-hour nickel hydrogen batteries are used as storage.
4. Thermal Control employs passive and active temperature control to optimise the performance of the spacecraft, their function depends on the available power and location of the satellite in space.
5. The structures system highlights the mechanical design of the spacecraft and how its integration of other subsystems enables the satellite to function efficiently. This subsystem determines the integration of the HRMA, ISIM and spacecraft module.
6. The propulsion system consists of a Momentum Unloading Propulsion Subsystem, which assists in station keeping and delta-V manoeuvres without causing excessive fuel consumption.
7. Flight system software is implemented to design algorithms for attitude determination, command, telemetry processing, thermal and electrical power control. This automated to allow engineers to remotely access the spacecraft mainframe.

An Electron Proton Helium Instrument (EPHIN) will be integrated to STABH as it is designed to obtain X-ray images of supernovae, SMBHs, active galactic nuclei and clusters of galaxies [8]. Chandra carries a particle

detector mounted near the HRMA that aids in monitoring the charged particle environment surrounding the satellite, this is done to protect the extremely sensitive equipment from particle radiation damage; this is particularly useful for STABH as the particle density near the SMBH is uncertain and it would be essential to protect the sensitive equipment and therefore increasing the lifespan of the satellite. Moreover, the combination of high angular resolution with low-noise focal plane detectors enables Chandra to obtain photon-limited, deep-field exposures of SMBHs [7]. These features will benefit STABH when orbiting SagA* as it will be able to distinguish the difference between the electromagnetic radiation emitted by a star and a black hole.

The James Webb Space Telescope (JWST/ Webb) is deemed the successor of the Hubble Space Telescope (HST/ Hubble). JWST is a near-infrared telescope with a payload of 6,190 kg orbiting Lagrange point 2 (L2), at altitudes of 250,000 km (periapsis) and 832,000 km (apoapsis) [9]. With 18 gold-plated beryllium hexagonal segments, Webb's 6.5 metre primary mirror is accompanied by a collection of infrared cameras and spectrometers, enabling the JWST to detect younger stellar objects and analyse the light speckles that Hubble does not have the ability for [10]. Hubble's limitation is due to distance of separation, the light from stellar bodies that reaches the Earth is stretched and morphed into the longer, red-shifted wavelengths that cannot be distinguished using optical telescopes. Hubble with a 2.4 metre Ultra-Low Expansion Glass® [11] optical telescope assembly consists of a faint object camera and spectrometer, a Goddard High- Resolution Spectrograph, a High-speed Photometer and a Wide-Field and Planetary Camera [12] [13]. HST, stationed at an altitude of 540 km has observational wavelengths extending from ultraviolet, visible light to near infrared [14], making it ideal for observing distant stars and planets within the solar system. The difference in primary mirror structure between the JWST and HST is illustrated in Figure 3.

Webb and Hubble require mechanical actuators to alter their mirrors' 3-dimensional alignment, they 'bend' to make small corrections to the structure and shape of the mirror to overcome minor distortion, but they are not powerful enough to modify the resolution of the image. In contrast, Chandra does not require actuators due to its reliance on collimators to increase the precision and accuracy of its observations. STABH is more closely related to Chandra's observational technology than it is to Webb and Hubble as it does not require actuators or segmented mirrors to function.

Webb's telescope and science module are cryogenically cooled to at least 40 °Kelvin to conduct near-infrared observations; a system of radiators, covered by the infamous five layer 'V' grooved sunshield, is used to passively cool down the satellite to its required operating temperature [15]. Active thermal control mechanisms are limited on Webb due to the incorporation of the deployable isolation tower [16] and Kapton sunshield [10]. Such an elaborate thermal control is not necessary for STABH as X-ray emissions at 1 million °Kelvin can be detected without relying on cryogenic cooling of scientific equipment.

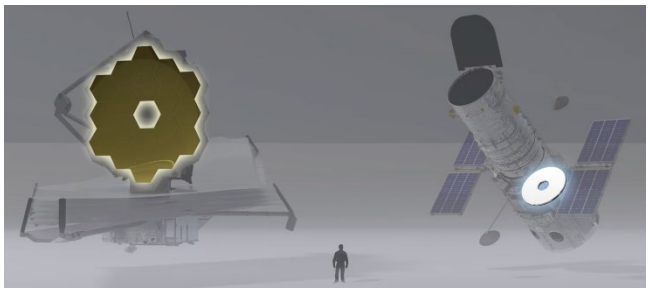

Figure 3. Structure comparison of the primary mirror sizes of Webb (left) and Hubble (right) [17].

Communication is done from the spacecraft bus through a high gain antenna using Kα bands at variable rates (7, 14 or 28 Mbps) and an omni-directional S-band antenna for emergency communications [10] at 16 (uplink) and 40 (downlink) Kbps. Furthermore, the Voyager space probes set out to flyby the Jovian and Saturnian systems, communicate with Earth at 170 Bps using S-band frequency and 115.2 Kbps at X-band frequency [18] [19], working collaboratively with the DSN ground systems. High efficiency antennas are used to downlink observational data to

DSN with the assistance of power and wave tube amplifiers to induce polarisation of the S-band and X-band frequencies, respectively [19] [20]. The dual output system is designed to maximise efficiency of data transmission as the spacecrafts operate for more than 50,000 hours; however simultaneous operation of S and X-band power amplifiers was restricted due to the excessive thermal load generation [19]. Omni-directional antennas are utilised as they provide near hemispherical transmission coverage, allowing Webb and the Voyagers to communicate with ground stations regardless of their orientation in space. The orientation of the satellite cannot be modified especially if it is in the process of observing a stellar body, the omni-directional antenna benefits the mission by acting independently on the satellite's position. This will be advantageous for STABH as it might not have the opportunity to reposition itself with the sole intent of conveying information back to Earth, thus causing the satellite to lose valuable observational data of the SMBH.

Five common types of rocket propellants include liquid, solid, hybrid, nuclear and electric [21]. Nuclear propulsion channels heat from a nuclear fission reaction into the liquid propellant chamber to generate thrust, they are theoretically capable of producing unrivalled quantities of thrust needed to propel STABH towards its designed orbit around SagA*. Nuclear propulsion was initially not considered for this project due to technological and political restrictions as it has minimum to no experimental proof. However, this project has taken its research opportunity to study nuclear propulsion [22] as well as antimatter propulsion due to their high energy densities. It was found that liquid and solid propellants release approximately 1 to 5 MJ of energy per kilogram of fuel whilst the nuclear fission reaction of Uranium-235 releases roughly 8×10^7 MJ/kg. Antimatter propulsion releases 9×10^{10} MJ/kg, which is almost 10 billion times higher than a simple chemical combustion reaction [23].

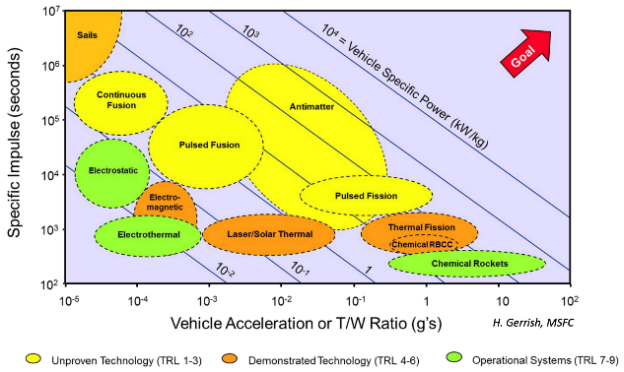

Figure 4. Propulsion landscape of operational, demonstrated and unproven propulsion systems [23].

Figure 4 depicts various operational, demonstrated, and unproven propulsion systems along with their specific impulses [23]. It is obvious that antimatter and nuclear (fusion and fission) propulsion produce a significantly higher specific impulse and therefore a higher spacecraft acceleration per kilogram of fuel. This research aims to further investigate the potential of utilising an antimatter propulsion system for STABH, particularly the implementation of a Proton-Antiproton Solid Core Engine ($I_{sp} \approx 900$ sec) or an Antiproton Catalysed Micro-fission/Fusion (ACMF) engine ($I_{sp} \geq 10,000$ sec) [23].

This paper focuses on observing black holes using X-ray spectroscopy, neither Webb nor Hubble contain the technology required to achieve this. Chandra, on the other hand, has produced a wide-field image of Messier 87*, but detailed polarised images of the SMBH were obtained by the Event Horizon Telescope which is a ground-based synchronised radio observatory network. As it is impossible to launch the EHT network into space, Chandra is the only deep space telescope that remotely reflects the mission requirements of STABH. This further justifies the need for a new spectrometric space telescope with a primary mission to study these gravitational powerhouses that control the structure of galaxies. The following methodology section consists of the theoretical research that was done to design the payload and bus subsystems of STABH, the Matlab and UE5 orbit simulations are also highlighted. The outcomes of the research and simulations are discussed in the results section, and a suitable conclusion is drawn.

2. Methodology

2.1.Orbital Design

The first step in determining the orbit of STABH is to calculate the necessary features of Sagittarius A*. From an astrophysics standpoint, Sagittarius A* was simplified and modelled as a point mass with a gravitation equalling that of 4.154 million $M_{\odot}$, as shown in the following equation. Sagittarius A* is known to have a radius of 17.249 $R_{\odot}$ (12011168.66 kilometres), the Schwarzschild radius of this SMBH is as calculated below.

$$M_{SMBH} = (4.145 \times 10^{6}) \times M_{\odot} = (4.145 \times 10^{6}) \times (1.989 \times 10^{30}) = 8.244 \times 10^{36}\ kgs$$

$$R_{Sch} = \frac{2G_N M_{SMBH}}{c^2} = \frac{2(6.67 \times 10^{-11})(8.244 \times 10^{36})}{3 \times 10^{8^2}} = 1.2198 \times 10^{10}\ m$$

Given a R_{Sch} value of 1.2198×10^{10} m, the altitude of 1 light-year can be measured either from the centre of the black hole or from the event horizon. Before the final satellite radius can be achieved, factors such as the force experienced by the satellite at various orbit radii must be calculated using $F_g = \frac{2G_N M_{SMBH} \times m}{R^2}$ where m is the mass of the satellite, approximated to be 8000 kg. Two force calculations were done (Table 1): the first case explores the gravitational attraction exhibited by the black hole from the event horizon to 1 light-year whereas the second case studies the force of gravity at a distance 1 light-year to 3 light-years away from the event horizon.

Table 1. Force cases based on orbital radii.

$\boldsymbol{F_g\ Case\ 1}$	$R_{Sch} < R < 9.461 \times 10^{15}\ m$
$\boldsymbol{F_g\ Case\ 2}$	$9.461 \times 10^{15}\ m < R < 2.8383 \times 10^{16}\ m$

The theoretical escape velocity for Sagittarius A* was calculated to be $3 \times 10^{8}\ m/s$, which is coincidentally equivalent to the speed of light. Changing the radius of orbit will change the velocity of the satellite, therefore also changing the orbital period and acceleration of the spacecraft. To address this concern, a range of orbit radii was chosen by creating an array of values with the minimum being 1 light-year (9.461×10^{15} m) and the maximum being 3 light-years (2.8383×10^{16} m). The acceleration, orbital velocity and period of the spacecraft was determined using the following equations and incorporating the aforementioned range of orbit radii.

$$V_{orbit} = \sqrt{\frac{G_N M_{SMBH}}{R}} \qquad T_{orbit} = \sqrt{\frac{4\pi^2 R^3}{G_N M_{SMBH}}} \qquad a_{satellite} = \frac{G_N M_{SMBH}}{R^2}$$

Orbit Simulation

Factors that influenced the orbital design of STABH include:

1. Gravitational force: an object is only pulled into the black hole singularity if it crosses the event horizon; satellites placed at any distance of separation before this threshold will experience sufficient force to stay in the orbit of the black hole without being overwhelmed into spaghettification.
2. Orbital velocity: the escape velocity of Sagittarius A* was calculated to be 3×10^{8} m/s. The satellite's orbit at different radii was determined.
3. Orbital period: the time taken to complete one orbit at different radii was compared to deduce the most efficient orbit radius.
4. Satellite acceleration: the centripetal acceleration of satellite was plotted for analysis.

Matlab calculations were completed using the previously mentioned physics equations and known astrophysical values of the Sagittarius A* SMBH. They were then implemented into the UE5 simulations to obtain results that were mathematically true.

STK and GMAT are common space simulation software that unfortunately have limited models of stellar objects and can only simulate planets, asteroids and the Sun within the solar system. The pre-existing stellar objects could not be modified to mimic a black hole. To overcome this challenge, Matlab and Unreal Engine 5 were utilised. The Sagittarius A* SMBH was simplified into a point mass with a radius of 1.2198×10^{10} m. Due to Matlab limit for allowable array sizes, the calculations were translated into the logarithmic scale which produced data points that were more manageable than the linear scale. The defining parameters of the black hole are listed in Table 2.

Table 2. Sagittarius A* SMBH parameters.

Parameter	True value (x)	Log(x)
R_{Sch}	1.2198×10^{10}m	23.2245 m
Satellite orbit radius – 1 LY	9.4610×10^{15}m	36.7860 m
Satellite orbit radius – 3 LY	2.8383×10^{16}m	37.8846 m
Image size	1×10^{50}	115.1293

The 'sphereVoxels' function in Matlab was used to create a logical 3-dimensional array that generated a sphere that can be modified using the x, y and z coordinates. Although black holes are invisible, their symmetrical structure was visualised using this method. Once the shape, size, magnitude and location of the black hole was defined, the orbit of STABH was plotted by setting various orbit radii and eccentricities. It was determined that the safest design would be to employ a circular orbit with the minimum altitude being greater than the Schwarzschild radius.

Black Hole Simulation

Unreal Engine 5 was utilised to simulate an interactive black hole where the completed satellite was later added to visually depict the size and structure of the outcome. UE5 is a game development software that can be easily configured to display the required structure of an object. Features including the Doppler effect and event horizon of the black hole were designed such that it presents a pseudo-realistic result. This simulation was supported by the theoretical calculations done in the previous section, thus producing a mathematically accurate SMBH. Figure 5 shows a flow chart of the methodology implemented to produce the Sagittarius A* SMBH and STABH's orbit in UE5.

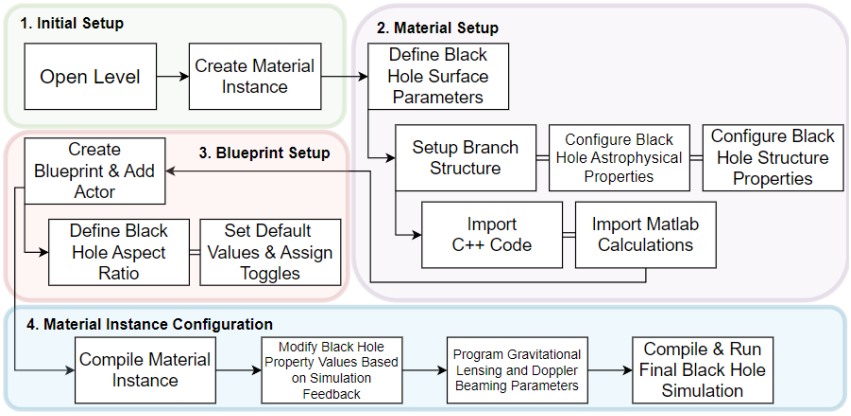

Figure 5. Overview flow chart of steps taken in UE5 to simulate a mathematically supported version of the Sagittarius A* supermassive black hole.

A material, blueprint and material instance are three layers within a UE5 level. Materials are used to define features of the object's surface such as texture, transparency, colour, and reflectivity by studying how light interacts with a surface [24]. This layer defines the external structure of the black hole including features such as the Doppler shift patterns and photon sphere colour. The blueprint is a node-based scripting system that creates gameplay elements which otherwise would require a multitude of programming [25]. C++ scripts were used to implement mathematical formulas to enhance the gameplay script and actuate the simulated object; the colour, shape, intensity and radius of the black hole to be modified using a tuner through the blueprint. Material instances create base parent material that can be customised to obtain different variations without compromising the foundational code [26]. "Inheritance" is used where desirable "features" of the parent is passed down to the children (material instances), these "features" are parameters such as Doppler intensity, photon ring intensity, Schwarzschild radius and so on.

2.2. Launch Vehicle Design

An analysis of the specific impulses of common rocket propellants revealed that liquid bipropellants have specific impulses ranging from 250 to 385 seconds whereas liquid monopropellants and solid fuels cap out around 250 seconds. The highest known specific impulse is a liquid oxygen/ liquid hydrogen combination propellant producing 455 seconds [27]. This project has taken this research opportunity to study nuclear propulsion [22] as well as antimatter propulsion due to their high energy densities.

Free radical propellants such as atomic hydrogen yield specific impulses ranging from 1200 - 1400 seconds [28] but are restricted due to their lack of stability. Present methods of free radical stabilisation are underdeveloped and propose a safety threat to humans as well as the instrumentation. Antimatter propellants are theorised to have specific impulses of 10^3 to 10^6 seconds [23]; however, a similar issue of stabilisation and storage arises once again. The respective specific impulses of Antiproton Catalysed Microfission/Fusion (ACMF), proton-antiproton (ρa) plasma core and beam core engines [23] [29] are tabulated below where it is evident that a high I_{sp} does not constitute a high thrust which is necessary to propel the rocket.

Table 3. Antimatter propulsion concepts and their specific impulses [23] [29].

Propulsion concept	I_{sp} (sec)	Thrust (N)	Exhaust Velocity (km/s)
ACMF	> 10,000	> 100,000	132.44
Proton-antiproton Plasma core (Hydrogen)	1000	5000	7840
Proton-antiproton Gas core	500	98,000	5
Proton-antiproton Solid core	900	90,000	9
Proton-antiproton Beam core	28×10^6	10	0.94 c

The data above provides sufficient proof that there needs to be a balance between the specific impulse, thrust and exhaust velocity of the rocket propellant. For further calculations, ACMF and plasma core engines will be disregarded. Although ρa beam core engines produce an unmatched specific impulse and an exhaust velocity close to the speed of light, it lacks thrust which could be detrimental when conducting transfer manoeuvres; both ρa gas and solid core engines have similar values.

Finally, the flight path of STABH from Earth to Sagittarius A* was determined by calculating the flight time and length of the journey using Einstein's theory of special relativity which states that as an object approaches the speed of light, it will experience time dilation, length contraction and mass dilation. The first two postulates are influenced by the rocket engine, therefore calculating the final rocket velocity and time of flight for the propulsion concepts will allow for the perfect engine selection.

2.3. Payload Configuration

It is crucial that STABH is designed to be capable of conducting observations of the Sagittarius A* SMBH in multiple wavelengths, Table 4 highlights the observational wavelength of various space telescopes where it is evident that the technology implemented in the Neil Gehrels Swift Observatory can be replicated for STABH. An observational wavelength ranging from X-ray, ultraviolet, visible light to infrared (0.12 nanometres to 160 micrometres) is intended for STABH.

Table 4. Observational wavelength of various space telescopes [30] [31] [32].

Space Telescope	Type	Observational Wavelength
Chandra X-ray Observatory	X-ray	0.12 nm - 12 nm
Hubble Space Telescope	UV, Visible light	90 nm - 2500 nm
James Webb Space Telescope	Near-infrared	0.6 μm - 5.3 μm
Spitzer	Infrared	24 μm - 160 μm
IXPE	X-ray	0.008 nm - 8 nm
Neil Gehrels Swift Observatory	Gamma, X-ray, UV, Visible light	<1 pm, 170 nm - 650 nm

STABH will be equipped with a device capable of studying the gravitational patterns surrounding a black hole, this can be achieved by either employing a employing a magneto-gradiometer or a gravimeter. A magneto-gradiometer measures the spatial changes of an object's field of gravity whereas a gravimeter detects the strength of the gravity field [33]. Bell Aerospace (now Lockheed Martin) developed a gravity gradiometer that employs four high-precision, room-temperature accelerometers [34] equi-spaced in a circle [35], their sensor axes tangential to the perimeter of the circle. Another potential magneto-gradiometer contender boasts a dodecahedral mount with six pairs of co-linear accelerometers [33] capable to measure variation in gravity in multiple dimensions.

Finally, an atomic clock twin is to be placed aboard the spacecraft with the other twin remaining on Earth. The aim is to replicate the 1971 Hafele–Keating experiment [36] where four Cesium-beam atomic clocks were placed in aircrafts that flew around Earth twice. When brought back to Earth, the clocks did not synchronise with one another; however, they supported the predictions of special relativity stating time dilates when travelling at velocities approaching the speed of light, the phenomenon known as kinematic time dilation. The Hafele–Keating experiment also studied the effects of gravitational time dilation [37] where it was suggested that the increase the gravitational potential energy causes the clocks to operate faster. As this experiment was conducted within the solar system with aircrafts travelling nowhere near $3x10^8$ m/s, the results obtained could be riddled with errors. So, placing one part of the twin atomic clock on STABH would help humankind understand the true potential of Einstein's theory of special relativity.

2.4. Bus Configuration

According to NASA [38], all spacecrafts depend on 8 basic bus subsystems: (1) Command & Data Handling, (2) Power Generation, Storage & Distribution, (3) Propulsion, (4) Thermal Control, (5) Guidance & Navigation (Attitude Control), (6) Telecommunications, (7) Structural Elements, (8) Micro-meteoroid Protection. Information regarding the bus/payload subsystems were obtained through space agency databases including NASA, ESA and JPL along with experimental publications.

Command & Data Handling

As the central nervous system of the spacecraft, the command and data handling (CDH) subsystem functions with three streams of information: the science data, engineering data and commands [39]. The science data is obtained by the payload which includes the multi-wavelength telescope, the atomic clock and the gravitational pattern detector.

"Health checks" of each subsystem is used to determine the progress and mission status, this is the engineering data. The command links are instructions sent to the spacecraft that controls its actions and functions. This is the data stream that requires the most attention as the entire mission can be jeopardised even with the smallest error whereas mistakes in the science and engineering streams can be rectified within a certain timeframe.

Webb, Hubble and Chandra return interferometric images at high data rates, as shown in Table 5. JWST located at L2 communicates in megabits per second whereas Voyager, although currently not transmitting science data, communicates with Earth in bits per second. It is evident that the distance between the spacecraft and ground will significantly influence the required data communication rate. STABH, situated 26,000 light-years away from Earth will have time-tagged commands and processes pre-loaded onto its computers as up/down-link communication with Earth will be limited unless it was to transfer science data.

Table 5. CDH data stream rates for different spacecrafts [9] [39].

Spacecraft	Command (up)	Science (down)	Engineering (down)
HST	1000 Bps	32 Kbps	4-32 Kbps
CXO	2000 Bps	32-1024 Kbps	64 Kbps
JWST	10 Mbps	57.2 Bps	8 Mbps
Voyager 1 & 2	16 Bps	Unavailable	40-1200 Bps

Power Generation, Storage & Distribution

Batteries were considered the primary source of electrical power in satellites but were limited in their longevity and temperature requirements for optimal performance, which lead to the development of solar energy based power systems. Radioisotope thermoelectric generators (RTGs) convert the radio-isotopic decay of elements into electrical energy power spacecrafts for a prolonged period without having to rely on a sun-source. Figure 6 shows that nuclear reactors can provide 10^3 to 10^7 Watts of power with an operating period of 1 hour to more than 10 years but are restricted due to safety and political reasons. RTGs have an output of 10^1 to $10^{3.5}$ Watts of power while operating anywhere from 6 months to more than 10 years whilst solar arrays can produce 10^4 Watts in a similar time frame.

Dual power systems combing RTGs and solar power are considered for STABH. Black holes as perfect black bodies will not emit any form of heat or light, limiting the use of solar energy as STABH's power source. While in orbit, STABH will have to rely on RTGs. Contrastingly, as STABH is travelling towards the black hole (post-separation from its launch vehicle), there is a higher possibility of achieving solar energy from passing-by stellar systems, this energy can be used to pre-emptively power the satellite. Various radioactive materials were considered for this mission by comparing their half-lives and energy released via decay, which follows Einstein's infamous mass-energy equation ($E = mc^2$), these are discussed in the results section.

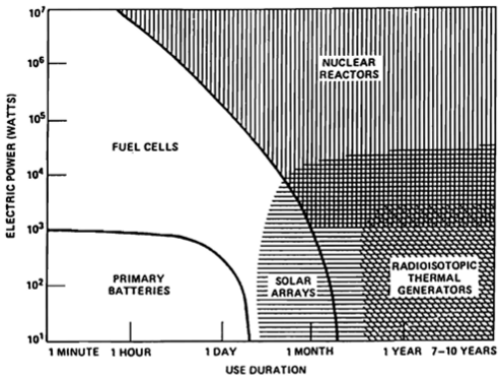

Figure 6. Operating duration of spacecraft power sources [39].

Propulsion

Common propulsion systems include cold-gas, mono-propellant, bi-propellant, dual-mode and solid motor systems, each with its own advantages and disadvantages depending on the mission requirements. Cold-gas, although inexpensive, has a very low specific impulse and thrust (typically less than 1 Newton) and therefore is not compatible for STABH. Mono-propellant systems supply steady thrust, a reasonable choice for attitude control in satellites. Bi-propellant systems are more complex and expensive, however produce a high specific impulse and thrust, making them ideal for high performance spacecrafts. Dual-mode propulsion systems are designed to satisfy both high impulse burns and low impulse attitude control pulses, they are ideal for spacecrafts that require frequent correctional thrusts during scientific observations to alter their trajectory and maintain the required orbit. Finally, solid motors are single burn systems suited for apogee kick burns but not correctional and attitude keeping pulses.

Monopropellants are cheaper than their competitors and are versatile with its correctional thrusts and station keeping pulses, its performance is medium at best. Bipropellants produce similar, maybe slightly better thrust results than monopropellants but at higher cost and complexity. Dual-modes are best suitable for planetary and deep space missions as they can combine a bi-propellant system's high energy correctional burn and a mono-propellant system's attitude control pulses into one package, designed specifically for orbit insertion and station keeping.

Tsiolkovsky's equation $\Delta v = g_0 I_{sp} \times ln\left(\frac{m_i}{m_f}\right)$ is used to obtain the delta-v of the rocket which is then used to calculate the thrust generated by a rocket [39] [27]. Thrust is generated as the rocket expels high pressure gas (produced by the combustion of propellants) at supersonic velocities through a converging- diverging nozzle. As a form of momentum exchange, the rocket propulsion is thermodynamically idealised to predict its performance; where the propellant gases are homogeneous, follow the perfect gas law with no friction at the nozzle walls and the flow is steady and constant with an axial velocity [39] [40].

Thermal Control

Electronic equipment have a narrow range of operational temperatures in which optimum efficiency is present, most materials tend to have a non-zero thermal expansion coefficient, such that when exposed to high temperatures they are subject to physical expansion and distortion [40]. All scientific equipment is initially designed and manufactured on Earth, where they operate at optimum efficiency at room temperature (20 to 25°C), however there are some exceptions. Computers and microprocessors operate at approximately -15°C to +50°C while momentum wheels and gyroscopes prefer temperatures between 0°C and +20°C; some elements within astronomical telescopes must be cooled to less than -7°C [40].

Space is subjected to four thermal conditions: direct solar radiation, albedo radiation, planetary radiation and spacecraft radiation (Figure 6). Since black holes are perfect black bodies, the first two forms of radiation are irrelevant. However, the acceleration of surrounding matter towards the black hole singularity produces heat which can be classified as planetary radiation, this will affect the thermal control design. It should be noted that since the existence and number of stellar objects near SagA* is unknown, an estimated value for the intensity of planetary cannot be determined as of now. Finally, the internal structure of STABH will also play a role in the thermal subsystem design as the heat generated by the scientific equipment must be transferred either to a different section of the satellite or to space.

Spacecraft radiation occurs in the infrared frequency [40], they are known as *grey bodies* that emit and absorb partial heat. The equilibrium temperature of the spacecraft $\left(T^4 = \frac{A_\alpha J_{incident}}{A_\varepsilon \sigma}\frac{\alpha}{\varepsilon}\right)$ depends on the solar absorptance-infrared emittance ratio ($\frac{\alpha}{\varepsilon}$) as the area of absorptance (A_α) and emittance (A_ε) along with the Stefan-Boltzmann constant (σ) can be treated as constants. The incident intensity *J* would also be constant as the emitting body does not vary. α and ε of the spacecraft surface and material will influence the overall needs for active and passive thermal control elements.

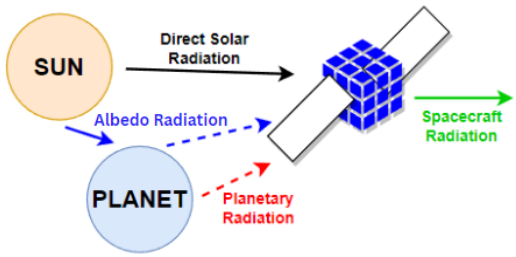

Figure 7. Space thermal environment showing direct solar, albedo, planetary and spacecraft radiations.

Passive thermal controls consist of the surface finishes of the spacecraft along with its insulative properties. Surface paints have deteriorative properties as they age, the telescope mirrors and solar arrays cannot be painted as this would restrict their functionality. Heat pipes and two-phase systems use volatile working fluids to transfer heat [39] [40], this requires a liquid with high heat wicking properties and is not suitable for a deep space mission like STABH where the behaviour of the fluid-vapour is unpredictable. Multi-layer insulation (MLI) blankets and phase change materials (PCM) are passive thermal control mechanisms that moderate the spacecraft's temperature during eclipse periods. MLI blankets can also act as radiation shields whereas PCMs are harder to navigate as sufficient free volume is needed to accommodate for the temperature dependant volume changes. The volume of this spacecrafts must be strictly adhered as there is no means of servicing during its mission, having a mercurial substance on-board is not a wise choice.

Active thermal control, albeit more complex than its passive counterpart, is more suited for equipment that is extremely temperature sensitive such as telescopes, scientific instruments and atomic clocks. Heaters exist in the form of metal co-axial cables with heating cores (thermo-coax) or metal-mounted resistors [40], they can be set to maintain a particular temperature required for optimum instrument function. Thermoelectric cooling is done through two phase heat pumps or Stirling-cycle coolers [40] which will most likely be used for the atomic clock and telescope aboard STABH. The aim is to implement an active temperature control system that does not rely on liquids or phase change substances as their behaviour in deep space environments remains uncertain.

Guidance & Navigation (Attitude Control)

Guidance and navigation (also referred to as attitude control) positions the spacecraft at the required location to obtain scientific measurements and telescopic images. Torque and momentum storage methods are used to orient the satellite based on its mission objectives; examples include pointing the solar arrays towards the sun, the thermal radiators towards space and the antennas towards the ground station. The eccentricity of the orbit will influence the angular momentum needed by the spacecraft to ensure that the sensors are pointed at their designated targets. Circular orbits such as the one designed for STABH does not require angular moment due to the local vertical of the spacecraft rotating at a constant rate of 1 revolution per orbit about the normal to the orbit plane [39] [40].

Attitude sensors detect disturbances in the satellite's orientation and communicates its torque demands with the onboard computers, torque controllers then work to realign the spacecraft based on the computer's directions. Magnetic and gravity gradients caused by the black hole as well as thrust misalignment would be the major cause of external torque disturbances for STABH. Internal torques impact the momentum between the moving parts of the satellite while external torque affects the total angular momentum [40]. Table 6 highlights the advantages and disadvantages of different torque control mechanisms.

Table 6. Advantages and disadvantages of different torques experienced by a spacecraft [40].

Torque type	Advantages	Disadvantages
Magnetic (external)	No fuel required, controllable torque magnitude	Altitude sensitive, causes magnetic interference
Gravity gradient (external)	No fuel required	Low accuracy, low torque, altitude sensitive
Reaction/ momentum wheels (internal)	Fine-pointing capability, momentum bias	Non-linear at zero speed
Control moment gyroscopes (internal)	Three-axis control, momentum bias	Reliability issues

The computation process is conducted using on-board computers, most satellites rely on ground control to provide detailed information regarding their positioning; however, this is not plausible for STABH. The attitude control system most appropriate for STABH based on its mission objectives is highlighted in the results section.

Telemetry

The telemetry system focuses on the transmission of the gathered data and commands, working collaboratively with the CDH system. Hardware involved in this subsystem include computers (to collect, process and store data), antennas and receivers (uplink information from ground including satellite orientation details and new mission aims), transmitters and amplifiers (downlink experimental data to ground). In most cases, data is sent back to Earth in a series of bits known as bytes (8 bits = 1 byte). An array of bytes (either kilo, mega, giga or tera) is sequentially transmitted to the ground station, this is considered raw data until further processing can be done. These values are determined by the satellite's data and link budgets.

The gathered analogue data from multiple subsystems sources including the payload are converted into digital packets, then through the process of time-division multiplexing, they are streamlined. Error detection is done through Cyclic Redundancy Checks codes which employs binary sequences.

To increase the efficiency of data transmission whilst reducing noise interference, two separate communication frequencies are often employed in satellites: one for payload information and the other for bus commands. S-band (2 to 4 GHz) and Ultra High Frequency (UHF) (350 to 450 MHz) are commonly used for payload and bus communications respectively. UHF is omni-directional, enabling the satellite to maintain a link with ground in any orientation, thus being effective in transmitting crucial commands. The S-band antenna is uni-directional and is usually on the nadir face of the satellite, more suited as a data transmission system to and from the payload. By integrating both UHF and S-band into a spacecraft, ground stations can maintain constant communication with the satellite, ensuring that no information is lost. STABH, situated 26,000 light-years from Earth has very minimum if not no possibility of maintaining constant contact with the grounds station, this makes the design process of a telemetry system for STABH more challenging.

Structural Elements

The structural elements of a spacecraft refer to its physical configuration and design. Three-axis stabilised spacecrafts have a "T" structure with the solar panels acting as branches, dual-spin satellites are cylindrical while CubeSats are designed in unit cubes. The structural components involve analysing various designs to obtain a spacecraft that can withstand static and dynamic loading experienced during testing and launch. The design process begins with configuration definition based on the mission objectives, material selection and manufacturing method selection. This paper took a more creative approach and simulated various spacecraft structures using Unreal Engine 5 (UE5) and the Space Station Creator extension.

An actor in UE5 is any object that can be added to a particular simulation level, these include static meshes such as spacecraft parts. Each component of the spacecraft (solar array, instrument module, etc.) needs to be

individually configured in terms of their dimensions, orientation and material. Once the static meshes are customised to their desired outcome, they are merged into actors that can be scaled to reflect the satellite's true size when positioned next to the simulated black hole (refer black hole simulation section). This will be done in the blueprint layer. Vertex Snapping is a feature that will be used to create the physical satellite structure by combining its subsystems and mechanical parts using the polygon vertices of static meshes. This will be further explored in the results section where unmerged meshes will be shown as well as the merged actors and their configuration.

Micro-meteoroid Protection

Micro-meteoroid protection aims to minimise the damage caused to spacecrafts in areas of high meteoroid flux. Asteroidal regions are common in solar systems and in deep space, however the terrain surrounding a black hole is uncertain and unpredictable, thus increasing the need for micro-meteoroid protection measures.

Failure modes caused by micro-meteoroid collisions include catastrophic rupture, leakage, vaporific flash, reduced structural strength and material erosion [41]. Multi-layer insulation (MLI) blankets, Kapton and Kevlar shielding, and other lightweight but dense fabrics are strong enough to reduce the impact of micro-meteoroids travelling at high velocities [41]. Another method is to set up warning systems with radio sensors on the spacecraft, this allows for a threat to be predicted beforehand, thus giving the spacecraft computers sufficient time to program the satellite to conduct collision avoidance manoeuvres.

3. Results and Discussion

3.1. Orbital Design

Figure 8 shows four Matlab plots that were obtained using the orbital equations mentioned previously. Figure 8A shows the gravitational force strength starting at the event horizon of the black hole, measured as the Schwarzschild radius, to 1 light-year. Five significant data points have been marked on the plot where a significant fall in gravitational force is seen at points 2 and 3. The exponential decay trend is obvious at data points 4 and 5 where the satellite will experience a force of 0.4821 and 0.04906 Newtons (respectively), proving that an object can be placed near the black hole before its event horizon. At an orbital radius of 1 light year, STABH will experience a gravitational force of 0.04906 N, travelling at a velocity of 7825.92 m/s and acceleration of 6.1322×10^{-6} m/s^2. However, if STABH is placed at an orbit of 3 light-years, it will experience a force of 0.005451 N, velocity of 40664.6 m/s and an acceleration of 6.8135×10^{-7} m/s^2. STABH's orbital periods are 240,866 and 139,064 years at radius of 1 and 3 light-years, respectively. The satellite is seen to have a higher velocity at a higher orbit radius; generally, increasing the orbit radius will decrease the velocity of the satellite due to their inverse relationship.

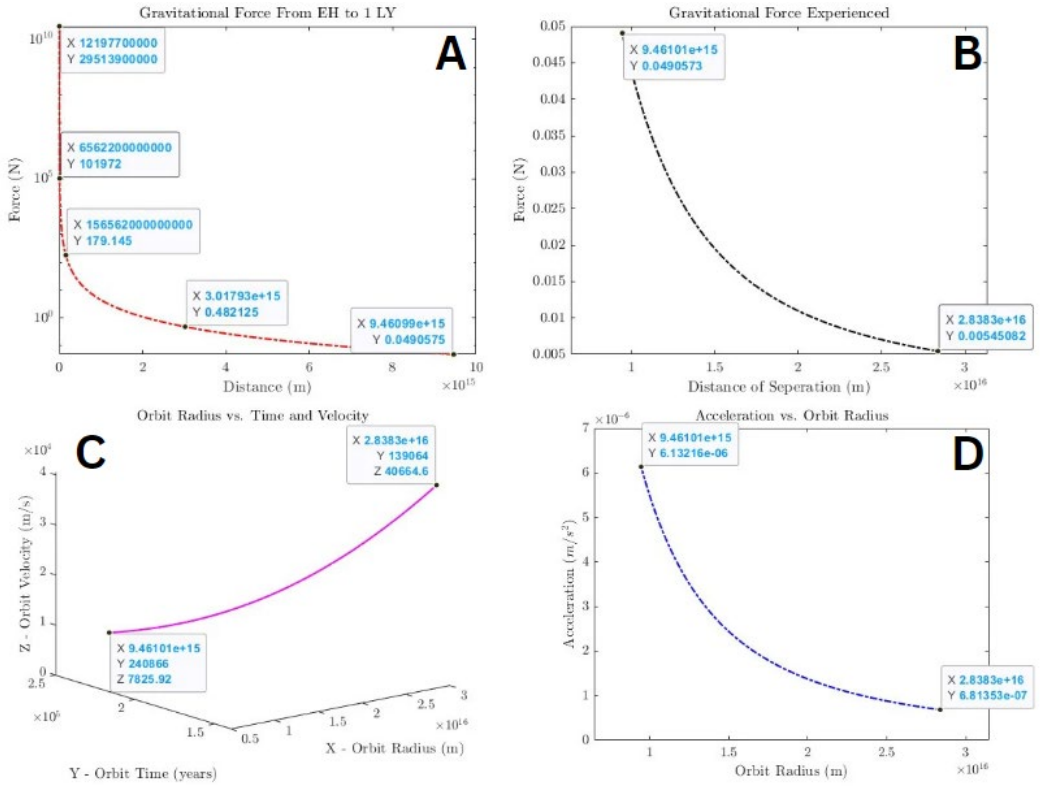

Figure 8. Matlab plots of STABH's orbit features. Figures 8A and 8B describe the gravitational force experienced at various orbital altitudes whereas Figures 8C and 8D show the satellite's orbit period, velocity and acceleration w.r.t its radius.

Orbit Simulation

Figure 9 depicts STABH's orbit around the Sagittarius A* SMBH. The orbit radii are plotted in the logarithmic scale (Table 6). The converted distance between 1 and 3 light-years in the log scale is 1.0986 m, however this value translates to 1.8922×10^{16} m. The natural log scale reduces the array size without altering the values, the true value can be recalled by using an exponential, the inverse function of log.

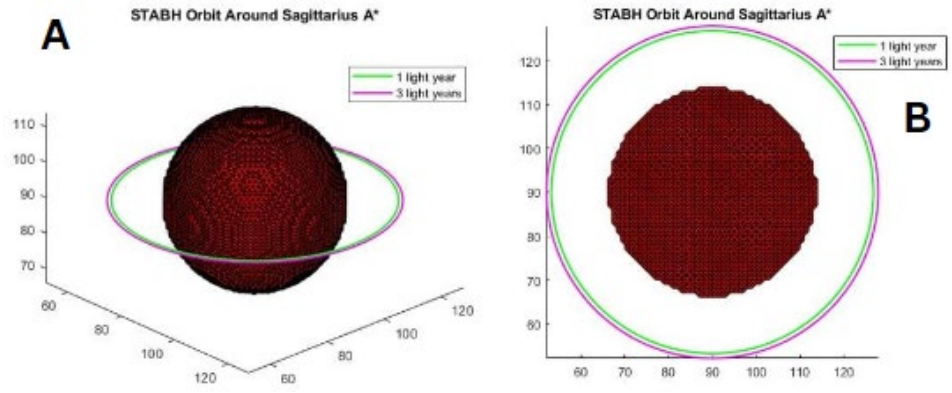

Figure 9. Matlab plots of STABH's orbit around SagA*. Figure 9A is the orbit structure at 45° and Figure 9B is the top view. The green line shows a radius of 1 light-year and the pink shows 3 light-years.

Black Hole Simulation

Although a game development software, UE5 has the necessary mathematical and physics encryption, the screenshot of the material instance file for SagA* is shown below. One of the issues in developing the script for SagA* was understanding the conversion factors between the true physical values and the values used in the software. This is because not all aspects were set to have a 1:1 conversion ratio due to the graphics and computational limits.

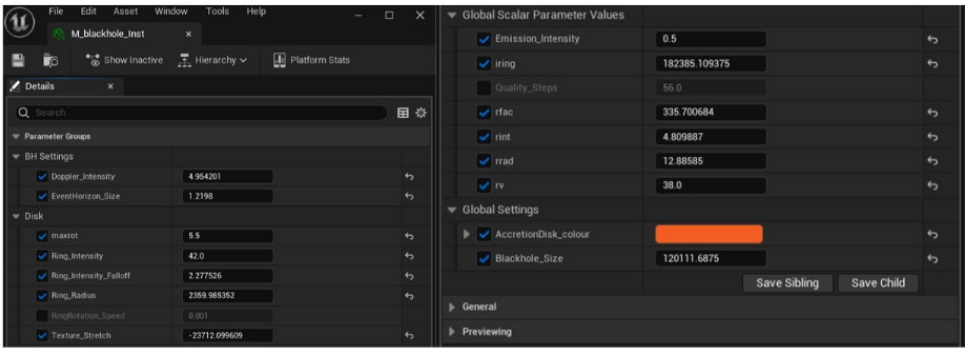

Figure 10. UE5 material instance of final black hole specification.

The scaling factors and conversion ratios were found by trial and error but once these values were locked, the total black hole can be scaled to any dimension while maintaining its mathematical proportions. Figure 11 depicts the result of the UE5 simulations with Figure 14C replicating the images captured by space telescopes. The simulated images of the Sagittarius A* supermassive black hole is consistent with the theory explained by Dr Kip Thorne during his talk at Cardiff University [42].

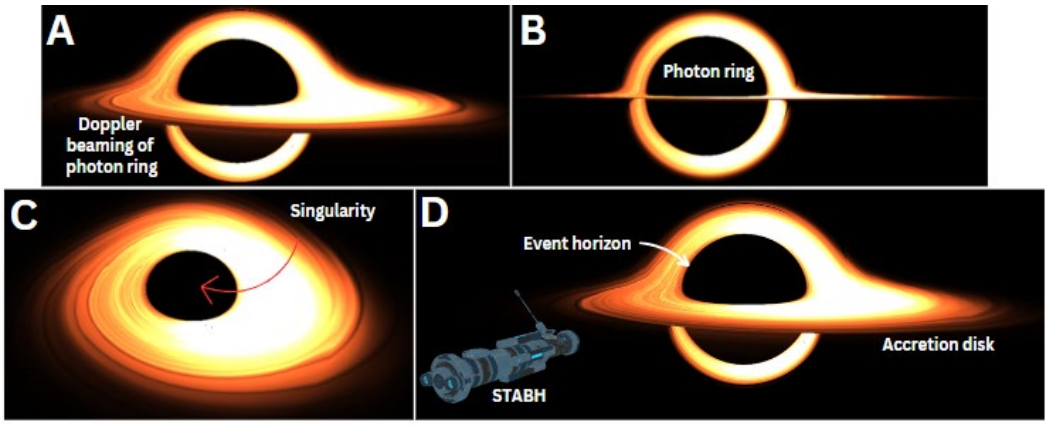

Figure 11. Annotated UE5 rendered images of the Sagittarius A* SMBH. Figure 11A is the 45° view, Figure 11B is the side and Figure 11C is the top view. Figure 11D shows STABH oriented to observe the black hole.

3.2.Launch Vehicle Design

The exhaust velocities were used to calculate the effect of time dilation and length contraction STABH would experience during its flight. The data tabulated below was calculated using Einstein's time dilation and length contraction equations. The aim was to calculate the dilated time and contracted distance that the spacecraft would experience. The true time of flight and distance of travel were 26,000 years and 2.459×10^{20} meters (respectively) as seen by an observer on Earth, outside the spacecraft's frame of reference. The shortest flight time is achieved by the ρα beam core engine that travels at 94% of the speed of light. The other engines do not have significant variance in flight time and distance, making ρα beam core engines the most viable form of propulsion.

Table 7. Special relativity features as affected by different launch vehicles.

Propulsion Concept	Exhaust Velocity (m/s)	Dilated Time (years)	Contracted Distance (m)
ρα Gas Core	5000	2.6×10^4	2.459×10^{20}
ρα Solid Core	9000	2.6×10^4	2.459×10^{20}
ρα Beam Core	0.94 c	8.8705×10^3	8.3924×10^{19}

3.3. Payload Configuration

The payload of STABH consists of three scientific instruments:

1. A deep space telescope with observational wavelengths in X-ray, ultraviolet and visible light with the addition of infrared, the intended wavelengths range from 0.12 nm to 160 μm.
2. A magneto-gradiometer (magnetometers) to measure the gravitational spatial changes of near a black hole.
3. An atomic clock twin with its counterpart situated at Earth to conduct observations of Einstein's theory special relativity by replicating the Hafele-Keating experiment.

STABH will focus on obtaining spectrographic images of the Sagittarius A* SMBH. X-ray spectroscopy aids in determining the temperature, density, elemental abundance, and ionisation stage of X-ray emitting bodies, allowing the black hole's accretion disk composition and temperature gradients to be analysed. Matter flow and turbulence near the accretion disk can be measured through the Doppler shifts. The Neil Gehrels Swift Observatory carries three separate telescopes: the Burst Alert, ultraviolet/ optical and X-ray telescope; a similar technology is intended for STABH. Although a cylindrical structure may limit the satellite's field of view, compared to the hexagonal primary mirror array of JWST, it will be sufficient for this mission. The structure of the primary mirror also aids in solidifying the spacecraft structure as it raises the potential for STABH to be constructed a dual-spin satellite. Orbiting Sagittarius A* at a radius of 1 and 3 light-years provides a field of view ranging from 43,633,231 to 137,604,667 kilometres; STABH will be able provide scientists with unprecedented data about black holes in wavelengths ranging from 0.12 nanometres to 160 micrometres (infrared, visible light, UV and X-ray).

Magneto-gradiometers are sensitive to magnetic fields produced by the spacecraft, so they are placed on extendable booms to reduce the risk of inaccurate data collection. Modifying the satellite structure is a small price to pay to obtain accurate and reliable gravity measurements. A search-coil magnetometer [43], weighing approximately 2kgs including the booms and cabling has been chosen for STABH. Copper coils are wound around a high magnetic permeability core with three orthogonal sensors to detect variations in magnetic patterns following Faraday's law of induction. Six pairs of co-linear accelerometers mounted on a dodecahedral fixture will allow STABH to detect low-frequency magnetic fluctuations and gravity patterns surrounding SagA*.

Finally, atomic clocks are the most accurate source of time telling as they study the internal resonance frequency between two hyperfine energy states of a chosen atom or molecule where their deflection translates to 1 second [44]. Table 8 shows the most common deep space atomic clocks along with their accuracy. Based on this mission's timeline, the Cesium-133 atomic-beam clock would produce the most accurate and reliable data. Besides conducting a properly calibrated version of the Hafele–Keating experiment, the atomic clock will also be used for Doppler tracking. This will advantageous due to the high Doppler shift patterns that exist around a black hole. Employing this equipment for STABH's mission will provide scientists with data on the behaviour of the black hole's photon ring as well as its interaction with the event horizon.

Table 8. Accuracy of different atomic clocks [45].

Atomic clock	Accuracy
Cesium-133	1 nanosecond / 1400000 years
Hydrogen Maser	0.45 nanoseconds / 12 hours
Rubidium Gas Cell	1.8 nanoseconds / 12 hours

3.1. Bus Configuration

Command & Data Handling

The command and data handling subsystem comprises of a computer, a command telemetry processor along with a memory and data storage device which is influenced by include (1) the orbit radius (variation in rotational speed), space radiation, (2) mission duration, (3) power requirements, (4) weight and size limitations, (5) computing power and (6) interface capabilities. STABH must possess sufficient computational power to self-direct as human intervention will be non-existent. STABH will employ the Ibeos EDGE 1U Payload Processor [46] along with the KP Labs Antelope on-board computer [47], specifications of both devices are shown in Table 9:

Table 9. Specifications of STABH's command and data handling system [46] [47].

CDH Component	CPU Clock Rate	RAM	Voltage	Operational Temperature	Radiation Tolerance
Ibeos EDGE 1U Processor	2 GHz	DDR3 2 Gb	< 5 Volts	-40 to 105 °C	30 kRad
KP Labs Antelope	300 MHz – 1.5 GHz	DDR4 1-2 Gb	5 Volts	-40 to 93 °C	20 kRad

The EDGE processor and Antelope on-board computer are designed for image acquisition and processing. Antelope can be configured to detect spatial threats like approaching micro-meteoroids and initiate trajectory corrective manoeuvres. This is an added feature to the micro-meteoroid projection mechanism. The radiation-tolerant structure of these components also make them a suitable choice for STABH as it orbits a black hole with unpredictable quantities of electromagnetic radiation.

Power Generation, Storage & Distribution

Since the nearest source of solar power near SagA* in unknown, using gallium arsenic or silicon solar cells for STABH is not recommended, instead Radioisotope Thermoelectric Generators (RTGs) have been chosen. Thermocouples convert the heat generated through the decay of radioactive elements into electrical energy which is then distributed throughout the spacecraft [48]. Strontium-90 (Sr-90), Curium-244 (Cm-244) along with its isotope Cm-245, Americium-241 (Am-241) and Plutonium-238 (Pu-238) are most common RTG radioisotopes with the latter being most employed in spacecrafts. The energy released per 1 gram of the previously stated radioisotopes are tabulated in Table 10.

Table 10. Specifications of radioactive elements used in RTGs [48].

Radioisotope	Pu-238	Cu-244	Cu-245	Sr-90	Am-241
Decay Type	Alpha	Alpha	Alpha	Beta	Alpha
Half-life	87.7 years	18.11 years	8250 years	28.8 years	432.2 years
Thermal Energy	12.22 W/g	120 W/g	3 W/g	0.95 W/g	114.7 mW/g

The thermal energy quotient must support the spacecraft demands whilst having a high half-life to reduce the mass of the radioactive element required. Cu-245 and Am-241 are not capable of releasing enough energy to power STABH whereas Sr-90 has a low half-life and undergoes beta decay which has a moderate ionising power and can

impact the performance of other subsystems. Although Cu-244 supersedes in thermal energy released, its half-life is restrictive, thus making Plutonium-238 most viable for STABH's prolonged mission despite its moderate thermal energy. Four general purpose heat source (GPHS) units will be integrated into the power subsystem. Each GPHS houses four iridium-clad ceramic Pu-238 fuel pellets weighing 1.44kg [48] and carrying 17.60kW of energy. STABH will therefore have 23.04kg of Plutonium-238 with 282kW of thermal energy. At an orbital radius of 1 light-year and an orbital period of 240,866 years, Pu-238 would consequentially go through 2746.5 half-lives.

Propulsion

A bi-propellant mixture like Webb's Secondary Combustion Augmented Thrusters (SCAT) using hydrazine (N_2H_4) and dinitrogen tetroxide oxidiser (N_2O_4) [49] is implemented in STABH, estimated to weigh between 8,000 and 10,000kgs. Given this mass, the thrusters used must be powerful enough to conduct station keeping as well as micro-meteoroid collision avoidance manoeuvres. The specifications of the 50N and 200N HPGP thrusters designed by Bradford ECAPS [50] [51] have been tabulated below. The 200N HPGP, although powerful, is heavier and requires more pre-heating power. Its capability of producing more than 4 times the thrust than the 50N HPGP makes it attractive for conducting sudden collision avoidance manoeuvres.

Table 11. Thruster specifications for Branford ECAPS 50N and 200N HPGP [50] [51] [52].

Thruster	Thrust Range	Specific Impulse	Pre-heating Power	Mass
50N HPGP	12.5 – 50 N	243 – 255 sec	75 – 100 W	2.1 kg
200N HPGP	55 – 220 N	243 – 255 sec	150 – 250 W	6 kg

Additionally, manoeuvring nozzles will be included due to their 50° swivelling ability [53]. Four of such nozzles are integrated, 2 on the posterior end for propulsion, one on the top and bottom surface of the spacecraft for orientation purposes. This is shown in the satellite design in the Structural Elements section.

Thermal Control

The temperature surrounding SagA* was found to be 1.4754×10^{-13} °Kelvin as seen in the equation below. STABH will need to generate sufficient heat to maintain optimum operating temperature of certain equipment rather than cooling them. The low environment temperature is beneficial for the telescope aperture as even the slightest heat gain can cause mirror distortion, but this will not affect the STABH telescope.

$$T_{SagA*} = \frac{\dot{h}c^3}{8\pi G_N M_{SMBH} k_B} = \frac{(1.0408 \times 10^{33})(3 \times 10^8)^3}{8\pi(6.67 \times 10^{-11})(8.244 \times 10^{36})(1.3806 \times 10^{-23})} = 1.4754 \times 10^{-13}\ °Kelvin$$

As STABH is in a region with minimum to no heat producing elements, active thermal technology is implemented to ensure that the payload is kept at its optimum operating temperature. This will be achieved using radioisotope heater units [54] as an extension of the RTG power source. Heat pumps along with variable conductance heat pipes would be highly beneficial as they work by moving non-condensable gas (usually nitrogen) throughout the satellite as a function of temperature gradients, enabling the precision of the temperature control to be modified within fractions of a degree [39]. Liquid loops and variable conductance heat pipes are not recommended as systems with volatile gases and liquid have uncertain behaviours [40], especially in an unserviceable spacecraft.

As for passive thermal control, the absorptance and emittance values of common surface finishes were studied. Polished Beryllium has a α/ε ratio of 44 [40] which is suitable for regions with low solar exposure, allowing the spacecraft to retain as much of the heat absorbed or generated as it can, reducing the use of heaters. The Optical Solar Reflectors have a α/ε ratio of 0.09 [40] as they need to constantly regulate their temperature to maintain a calculated equilibrium. If the telescopes absorb too much heat and are unable to dissipate it, they risk distorting the mirror arrays,

causing the observations made to be inaccurate. MLI blankets and aluminised plastic film will be used to retain excess heat energy.

Guidance & Navigation (Attitude Control)

Star sensors have accuracies of 1 arc second and better. Three-axis stabilised spacecrafts employ star trackers and mappers as their field of view can monitor several stars to obtain a more accurate location. Star scanners are more suited for spinning spacecrafts as the rotational movement allows them to scan the sky efficiently [40]. STABH will most likely use a combination of star scanners and trackers to orient itself. The Hydra APS star sensor, operating at 11 Watts at 20°Celsius [40] has three optical sensors integrated into one fixture and it can track 15 stars simultaneously.

Three orthogonal gyroscopes measure the x, y and z inertial angular velocities of the spacecraft [40] to determine its three-dimensional coordinates including its skew angle. The Ring Laser Gyroscope consists of ceramic triangular prisms that split the laser at one vertex such that two streams of lasers are reflected internally in opposing directions. The rotation of the prism causes fluctuations in the interference patterns of the two laser streams, allowing the guidance and navigation system to calculate the change in inertial angular momentum. Attitude control can also be directed using magnetometers. Although already present in STABH, attitude control will not be the primary use of the magnetometer as minor variations in the magnetic field can cause discrepancies in coordinate determination [40] [43].

Telemetry

S-band (2 to 4 GHz) frequency is utilised for payload data transmission and UHF (350 to 450 MHz) is used for bus commands. By implementing two transmission rates, the satellite can reduce noise interference and maintain contact with ground. Unfortunately, this scenario does not apply to STABH as it is located 26,000 light-years from Earth, leading it to have very limited communication with the ground station network. Even though UHF antennas have omni-directional transmission beams, the issue lies in the distance of separation between STABH and Earth along with the time taken for commands and data to reach their respective recipients. With current limited technology, the telemetry system for STABH cannot be conclusively determined. However, there exists a possibility to design an array of satellites that form a constellation, acting as bridges for the science and engineering data to travel between STABH and the ground station network in the future.

Structural Elements

UE5's Space Station Creator (SSC) extension allows developers to create structures that replicate the real features of spacecrafts. SSC has five actor configurations features: maps, textures, materials, meshes and blueprints. Maps and textures are not applicable as they control animations. Meshes can be configured in size, structure, colour and scale with respect to neighbouring meshes, useful for modifying spacecraft parts like telescopes, RTGs, onboard engines and instrument modules. Materials alter the surface finishes and aesthetic features. Blueprints were used to make the designed spacecraft interact with stellar objects; they can also be translated into C++ scripts.

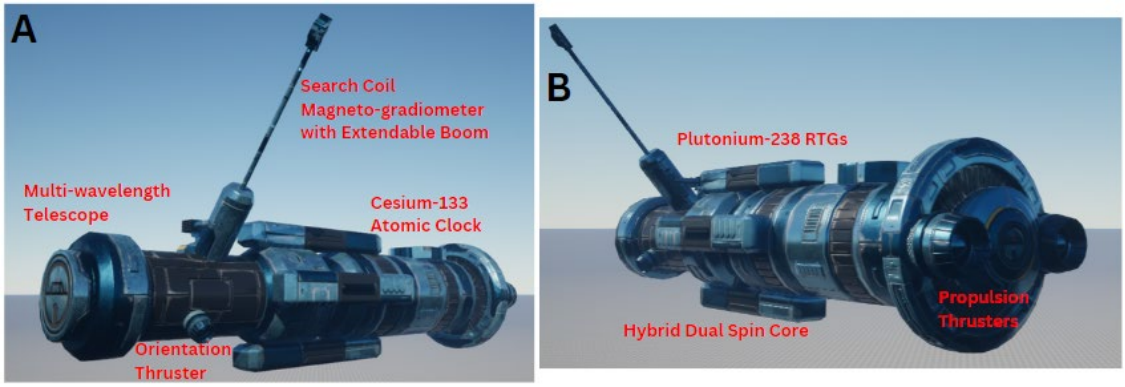

Figure 12. Annotated rendered images obtained through Unreal Engine 5 and Space Station Creator. Figure 12A shows the structure of STABH as seen at 45° whereas 12B shows the posterior view with the propulsion thrusters.

Figure 12 depicts the structure of STABH and the Sagittarius A* SMBH generated using UE5 with annotated features. The magneto-gradiometer attached to an extendable boom is kept away from the main structure of the satellite to analyse the gravity patterns without being affected by magnetic interference. The multi-wavelength telescope has a meteoroid protection shield which prevents the mirror arrays from being damaged. Two orientation thrusters are included (only one is visible), the other is located on the flip side of the spacecraft; two propulsion thrusters are located posterior to STABH. Four Plutonium-238 RTGs surround STABH whilst the Cesium-133 atomic-beam clock is mounted onto STABH such that it is least affected by the satellite's excess heat production. Figure 10B, achieved through blueprint configurations, shows STABH oriented towards the SagA* SMBH, the two posterior propulsion thrusters can be seen from this angle.

Micro-meteoroid Protection

The micro-meteoroid protection mechanisms implemented in STABH are multi-layer insulation (MLI) blankets as cushioning during minor asteroid collisions, Kapton and Kevlar protecting shielding to increase the structural integrity of the satellite while remaining lightweight [41], and the integration of micro-meteoroid detection sensors that allow the satellite computers to predict collisions threats beforehand. The micro-meteoroid detection system would work collaboratively with the on-board propulsion engines to execute collision avoidance manoeuvres to prevent the satellite from experiencing catastrophic ruptures and structural damage to the scientific instruments.

4. Conclusion

Current technology limits humankind from conducting direct research with black holes due to their invisibility, indirect investigations are done by analysing the heat-sourced X-ray emissions generated by the acceleration of surrounding matter towards the black hole singularity. To overcome this, a hypothetical deep space satellite was designed to analyse the Sagittarius A* supermassive black hole while orbiting it. The payload and bus configurations were determined by studying various deep space satellites including the Chandra X-ray Observatory, James Webb and Hubble Space Telescopes as well as the Voyager space probes.

The Satellite That Analyses Black Holes (STABH) carries a multitude of scientific equipment that will expand the knowledge surrounding black holes and by extension the creation of the universe. The multi-wavelength telescope can produce spectrographic images of the SagA* in infrared, visible light, ultraviolet and X-ray frequencies. When these images are combined, they can show features of the black hole that were previously unknown. The integrated Cesium-133 atomic-beam clock not only allows scientists to conduct an accurate version of the Hafele-Keating experiment testing the theory of relativity, it can also study the Doppler shift of the Sagittarius A*'s photon ring. Thus, providing humankind with unprecedented knowledge on the black hole's behaviour and the event horizon's interaction

with surrounding matter. Furthermore, a search coil magnetometer is implemented to measure the spatial changes of a black hole's field of gravity. This is done so that scientists can map the gravitational wave patterns exuded from the black hole and make relativistic observations on how this influences the orientation and structure of the galaxy.

As for the bus system configuration, a hybrid dual-spin spacecraft with four Plutonium-238 RTGs, carrying 2 propulsion thrusters and 2 orientation stabilising thrusters (each with 50° manoeuvring nozzles) was designed. STABH is designed with EDGE 1U Payload Processor developed by Ibeos in collaboration with the KP Labs' Antelope on-board computer as its command and data handling system. Radioisotope heater units are fixed such that the equilibrium temperature of the scientific equipment is maintained as the space environment surrounding a black hole is extremely cold due to the lack of solar waves. Hydra APS Star Sensors and internalised Ring Laser Gyroscopes are used for attitude control as they work together with the on-broad engines to stay on course and conduct micro-meteoroid avoidance manoeuvres. The structural features of STABH were simulated using the Space Station Creator extension in Unreal Engine 5.

Finally, the orbit structure of STABH around the Sagittarius A* SMBH was determined using Matlab. The orbital velocities, period, acceleration, and gravitational force experienced with respect to the orbit radius was calculated and studied. Unreal Engine 5 was utilised to simulate a mathematically supported model of the Sagittarius A* SMBH, the known physics of the black hole's behaviour was simulated as best as possible.

This paper hopes to have provided the scientific and engineering community with the foundation to materialise a deep space satellite that can investigate the cosmic implications initiated by the gravitational pull of a supermassive black hole.

5. Acknowledgements

Thank you to Dr Manuj Awasthi, my incredible research thesis supervisor, for his infinite knowledge, patience and guidance. Special thanks to Shane Hengst, the wonderful astrophysics consultant from CSIRO for his time and support.

6. References

[1] K. Akiyama, A. Alberdi, W. Alef, J. C. Algaba, R. Anantua, K. Asada, R. Keiichi, U. Bach, A. Baczko and D. Ball, "First M87 Event Horizon Telescope results. IV. Imaging the central supermassive black hole," *The Astrophysical Journal Letters,* vol. 930, no. 2, 2019. https://doi.org/10.3847/2041-8213/ab0e85.

[2] EHT, "Astronomers Reveal First Image of the Black Hole at the Heart of Our Galaxy," [Online]. Available: https://eventhorizontelescope.org/blog/astronomers-reveal-first-image-black-hole-heart-our-galaxy. [Accessed 14 August 2023].

[3] NASA, "Chandra Captures X-rays in Coordination with Event Horizon Telescope," 2019. [Online]. Available: https://chandra.harvard.edu/photo/2019/black_hole/. [Accessed 14 August 2023].

[4] E. S. Observatory, "A view of the M87 supermassive black hole in polarised light," March 2021. [Online]. Available: https://www.eso.org/public/images/eso2105a/. [Accessed 14 August 2023].

[5] C. Bambi, "Astrophysical Black Holes: A Review," in *Multifrequency Behaviour of High Energy Cosmic Sources - XIII*, 2019. https://doi.org/10.22323/1.362.0028.

[6] C. Reynolds, "Measuring black hole spin using X-ray reflection spectroscopy," in *The Physics of Accretion onto Black Holes*, Springer, 2013. https://doi.org/10.1007/s11214-013-0006-6, pp. 277-294.

[7] B. Wilkes and W. Tucker, The Chandra X-ray Observatory, IOP Publishing Limited, 2019.

[8] M. Weisskopf, H. Tananbaum, L. V. Speybroek and S. O'Dell, "Chandra X-ray Observatory (CXO): Overview," *X-Ray Optics, Instruments, and Missions III,* vol. 4012, no. SPIE, pp. 2-16, 2000. https://doi.org/10.1002/0471263869.sst072.

[9] P. Sabelhaus and J. Decker, "An overview of the James Webb space telescope (JWST) project," *Optical, Infrared, and Millimeter Space Telescopes,* vol. 5487, pp. 550-563, 2004. https://doi.org/10.1117/12.549895.

[10] P. Sabelhaus, D. Campbell, M. Clampin, J. Decker, M. Greenhouse, A. Johns, M. Menzel, R. Smith and P. Sullivan, "Overview of the James Webb Space Telescope (JWST) project," *UV/Optical/IR Space Telescopes: Innovative Technologies and Concepts II,* vol. 5899, pp. 241-254, 2005. https://doi.org/10.1117/12.612659.

[11] A. Gianopoulos, "Observatory - Hubble vs. Webb," NASA, May 2022. [Online]. Available: https://www.nasa.gov/content/goddard/hubble-vs-webb-on-the-shoulders-of-a-giant. [Accessed 14 August 2023].

[12] R. Polidan, "Hubble Space Telescope Overview," in *29th Aerospace Sciences Meeting*, 1991. https://doi.org/10.2514/6.1991-402.

[13] L. Endelman, "Hubble Space Telescope: mission, history, and systems," in *19th Intl Congress on High-Speed Photography and Photonics*, SPIE, 1991, pp. 422-441.

[14] M. Belleville and B. Dunbar, "About The Hubble Space Telescope," NASA, 2022. [Online]. Available: https://www.nasa.gov/mission_pages/hubble/about. [Accessed 14 August 2023].

[15] J. Nella, P. Atcheson, C. Atkinson, D. Au, A. Bronowicki, E. Bujanda, A. Cohen, D. Davies, P. Lightsey and R. Lynch, "James Webb Space Telescope (JWST) observatory architecture and performance," in *Optical, Infrared, and Millimeter Space Telescopes*, SPIE, 2004, pp. 576-587.

[16] M. Clampin, "Recent progress with the JWST Observatory," *Space Telescopes and Instrumentation 2014: Optical, Infrared, and Millimeter Wave,* vol. 9143, 2014. https://doi.org/10.1117/12.2057537.

[17] "Comparison: Webb vs Hubble Telescope," NASA, [Online]. Available: https://www.jwst.nasa.gov/content/about/comparisonWebbVsHubble.html. [Accessed 14 August 2023].

[18] C. Kohlhase and P. Penzo, "Voyager mission description," *Space Science Reviews,* vol. 21, pp. 77-101, 1977. https://doi.org/10.1007/BF00200846.

[19] R. Ludwig and J. Taylor, "Voyager telecommunications," in *Deep Space Communications*, Wiley Online Library, 2016, pp. 37-33.

[20] E. Posner and R. Stevens, "Deep space communication-Past, present, and future," *IEEE Communications Magazine,* vol. 22, pp. 8-21, 1984. https://doi.org/10.1109/MCOM.1984.1091955.

[21] P. A. Ritter, Optimization and Design for Heavy Lift Launch Vehicles, Tennessee Research and Creative Exchange, 2012.

[22] O. Muránsky, "Nuclear propulsion systems," ANSTO, [Online]. Available: https://www.ansto.gov.au/our-science/nuclear-technologies/reactor-systems/nuclear-propulsion-systems. [Accessed 14 August 2023].

[23] M. LaPointe, "Antimatter Propulsion," 2020. [Online]. Available: https://ntrs.nasa.gov/api/citations/20200001904/downloads/20200001904.pdf. [Accessed 14 August 2023].

[24] U. Engine, "Unreal Engine 5.1 Materials," 2023. [Online]. Available: https://docs.unrealengine.com/5.1/en-US/unreal-engine-materials/. [Accessed 14 August 2023].

[25] U. Engine, "Introduction to Blueprints," 2023. [Online]. Available: https://docs.unrealengine.com/5.1/en-US/introduction-to-blueprints-visual-scripting-in-unreal-engine/. [Accessed 14 August 2023].

[26] U. Engine, "Creating and Using Material Instances," 2023. [Online]. Available: https://docs.unrealengine.com/5.1/en-US/creating-and-using-material-instances-in-unreal-engine/. [Accessed 14 August 2023].

[27] H. Curtis, Orbital Mechanics For Engineering Students, Elsevier Butterworth-Heinemann, 2015.

[28] P. Atkinson, "Outer space Propulsion Using Nuclear Energy, hearings before subcommittees of the Joint Committee on Atomic Energy," *Congress of the United States 85th Cong.,* p. 145, 1958.

[29] R. Forward, "Antiproton annihilation propulsion," *Journal of Propulsion and Power,* vol. 1, no. 5, pp. 370-374, 1985. https://doi.org/10.2514/3.22811.

[30] NASA, "Observatories Across the Electromagnetic Spectrum," 2013. [Online]. Available: https://imagine.gsfc.nasa.gov/science/toolbox/emspectrum_ observatories1.html. [Accessed 14 August 2023].

[31] CalTech, "Space Telescopes," CalTech University, 2015. [Online]. Available: https://cosmos.astro.caltech.edu/page/telescopes. [Accessed 14 August 2023].

[32] P. Observatory, "Publications of French Observatories," 2023. [Online]. Available: https://bibnum.obspm.fr/perios-obs. [Accessed 14 August 2023].

[33] J. Suter, P. Zucker and P. Martin, "Precision Accelerometers for Gravity Gradient Measurements," *Johns Hopkins APL Technical Digest,* vol. 15, no. 4, pp. 347-352, 1999.

[34] D. DiFrancesco, A. Grierson, D. Kaputa and T. Meyer, "Gravity gradiometer systems--advances and challenges," *Geophysical Prospecting,* vol. 4, pp. 615-623, 2009. https://doi.org/10.1111/j.1365-2478.2008.00764.x.

[35] J. Lee, "FALCON gravity gradiometer technology," *ASEG Extended Abstracts,* vol. 2001, no. 1, pp. 1-4, 2001. https://doi.org/10.1071/EG01247.

[36] W. Rodrigues and E. de Oliveira, "A comment on the twin paradox and the Hafele-Keating experiment," *Physics Letters A,* vol. 140, no. 9, pp. 479-484, 1989. https://doi.org/10.1016/0375-9601(89)90126-6.

[37] D. Koks, Explorations in mathematical physics: the concepts behind an elegant language, Springer, 2006.

[38] D. Murfet, "Spacecraft and Platform Subsystems," [Online]. Available: https://sbir.nasa.gov/printpdf/56609#:~:text=A%20spacecraft%20bus%20is%20made,%2Fsoftware%3B%20and%20structural%20elements. [Accessed 14 August 2023].

[39] C. D. Brown, Elements of Spacecraft Design, American Institute of Aeronautics and Astronautics. Inc, 2002.

[40] P. Fortescue, G. Swinerd and J. Stark, Spacecraft System Engineering, John Wiley & Sons Ltd, 2011.

[41] NASA, "Micrometeoroid Protection," [Online]. Available: https://llis.nasa.gov/lesson/705. [Accessed 14 August 2023].

[42] K. Throne, *The Warped Side of the Universe: Kip Thorne at Cardiff University,* Cardiff University, 2020.

[43] NASA, "Themis - Search Coil Magnetometer (SCM)," 2007. [Online]. Available: https://www.nasa.gov/mission_pages/themis/spacecraft/SCM.html. [Accessed 14 August 2023].

[44] W. M. Itano, "Atomic Clocks," 2021. [Online]. Available: https://www.accessscience.com/content/article/a060100. [Accessed 14 August 2023].

[45] ESA, "Galileo's clocks," 2023. [Online]. Available: https://www.esa.int/Applications/Navigation/Galileo/Galileo_s_clocks #:~:text=The%20passive%20hydrogen%20maser%20clock,0.45%20nanoseconds%20over%2012%20hours. [Accessed 14 August 2023].

[46] SatSearch, "EDGE 1U Payload Processor," [Online]. Available: https://satsearch.co/products/ibeos-edge-1u-payload-processor. [Accessed 14 August 2023].

[47] SatSearch, "Antelope On-board computer," [Online]. Available: https://satsearch.co/products/kplabs-antelope. [Accessed 14 August 2023].

[48] World Nuclear Association, "Nuclear Reactors and Radioisotopes for Space," 2021. [Online]. Available: https://world-nuclear.org/information-library/non-power-nuclear-applications/transport/nuclear-reactors-for-space.aspx. [Accessed 14 August 2023].

[49] L. Meza, F. Tung, V. Spector, T. Hyde and S. Anandakrishnan, "Line of Sight Stabilization of James Webb," NASA, [Online]. Available: https://ntrs.nasa.gov/api/citations/20050139747/downloads/20050139747.pdf. [Accessed 14 August 2023].

[50] SatSearch, "50N HPGP Thruster," [Online]. Available: https://satsearch.co/products/ecaps-50n-hpgp-thruster. [Accessed 14 August 2023].

[51] SatSearch, "200N HPGP Thruster," [Online]. Available: https://satsearch.co/products/ecaps-200n-hpgp-thruster. [Accessed 14 August 2023].

[52] NASA, "In-space Propulsion," 2022. [Online]. Available: https://www.nasa.gov/smallsat-institute/sst-soa/in-space-propulsion. [Accessed 14 August 2023].

[53] T. Wang, A. Lidtke, F. Giorgio Serchi and G. Weymouth, in *Manoeuvring of an aquatic soft robot using thrust-vectoring*, IEEE Xplore, 2019, pp. 186-191.

[54] NASA, "Light-Weight Radioisotope Heater Unit | Thermal Systems – NASA RPS: Radioisotope Power Systems," [Online]. Available: https://rps.nasa.gov/power-and-thermal-systems/thermal-systems/light-weight-radioisotope-heater-unit/. [Accessed 14 August 2023].